Quantum transport in three-dimensional metalattices of platinum featuring an unprecedentedly large surface area to volume ratio

Yixuan Chen, Yunzhi Liu, Parivash Moradifar, Andrew J. Glaid, V, Jennifer L. Russell, Pratibha Mahale, Shih-Ying Yu, Tyler E. Culp, Manish Kumar, Enrique D. Gomez, Suzanne E. Mohney, Thomas E. Mallouk, Nasim Alem, John V. Badding, and Ying Liu

Phys. Rev. Materials **4**, 035201 — Published 30 March 2020

DOI: 10.1103/PhysRevMaterials.4.035201

Quantum Transport in Three-Dimensional Metalattices of Platinum Featuring an Unprecedentedly Large Surface Area to Volume Ratio

Yixuan Chen[1,6], Yunzhi Liu[2,6], Parivash Moradifar[3,6], Andrew J. Glaid V[2,6], Jennifer L. Russell[2,6], Pratibha Mahale[2,6], Shih-Ying Yu[4,6], Tyler E. Culp[4,6], Manish Kumar[4,6], Enrique D. Gomez[3,4,6], Suzanne E. Mohney[4,6], Thomas E. Mallouk[1,2,3,6], Nasim Alem[3.6], John V. Badding[1,2,3,6,a], Ying Liu[1,6,a]

[1]*Department of Physics, Pennsylvania State University, University Park, PA 16802, USA.*

[2]*Department of Chemistry, Pennsylvania State University, University Park, PA 16802, USA.*

[3]*Department of Materials Science and Engineering, Pennsylvania State University, University Park, PA 16802, USA.* [4]*Department of Chemical Engineering, Pennsylvania State University, University Park, PA 16802, USA.*

[5]*Department of Biochemistry and Molecular Biology, Pennsylvania State University, University Park, PA 16802, USA.*

[6]*Materials Research Institute, Pennsylvania State University, University Park, PA 16802, USA.*

Three-dimensional (3D) electronic nanomaterials are less explored than their counterparts in the lower dimensions because of the limited techniques for the preparation of high-quality materials. Here we report characterization of and quantum transport measurement on 3D metalattices of Pt grown in the voids of self-assembled templates of silica nanospheres by confined chemical fluid deposition. These Pt metalattices featuring an unprecedentedly large surface area to volume ratio were found to show positive magnetoresistance (MR) at low temperatures, changing from being positive to negative in low magnetic fields within a narrow temperature window as the temperature was raised. The low-field MR was attributed to the effect of quantum interference of electronic waves in the diffusive regime in 3D, processes known as the weak localization and antilocalization, which have not been observed previously in any 3D form of Pt. We argue that the presence of the large surface area to volume ratio results in such a strong enhancement in the electron-phonon scatterings that a change in the sign in the MR is enabled.

PhySH:

Research Areas: Condensed matter and material physics, transport phenomena, localization, weak localization.

Physical Systems: 3-dimensional systems, complex materials, metamaterials.

[a] Authors to whom correspondence should be addressed.

Experimental Techniques: Sample preparation, chemical synthesis; Transport techniques, resistivity measurements.

Three-dimensional (3D) electronic nanomaterials, which are in general more difficult to prepare than their lower-dimensional counterparts because certain nanofabrication tools such as e-beam lithography are not applicable, have attracted a great deal of interest in recent years originating from both scientific and technological considerations. 3D nanomaterials of Pt, which have hardly been studied, are expect to possess a fascinating combination of material properties including for example very strong spin-orbital coupling, incipient ferromagnetism, and a large electron-phonon interaction [1-5]. Its large atomic number, Z, of 78, makes its spin-orbital coupling large, which has an effect even on its effectiveness as a catalyst [6]. The material itself is also a popular choice for spintronics applications [1, 2]. Among all non-magnetic elemental metals, Pt features one of the largest exchange-enhanced Pauli susceptibilities with a Stoner enhancement factor of 3.9 [3], which makes it nearly ferromagnetic. Its electron-phonon coupling constant, λ, is also very large, featuring a value of 0.66 estimated from resistivity and 0.31 from specific heat data [4]. Even though such a large λ value should favor superconductivity, measurements down to an electronic temperature of 1.5 μK, the lowest temperature achieved in solids thus far, uncovered no indication of superconductivity [5]. It is suggested that the strong ferromagnetic fluctuation inhibits superconductivity even though it is not strong enough to trigger a ferromagnetic instability.

The surface of Pt was found to strongly modify its properties. Nanoclusters or nanowires of Pt possess extraordinary magnetic polarization, leading for example to spontaneous spin-polarized transport in Pt nanowires [3]. Nanomaterials of Pt also exhibit enhanced chemical activity for oxygen reduction [6]. Most interestingly, superconductivity is observed in compacted Pt powder with an average grain size in the micron range [7] and a transition temperature of $T_c \approx 1.5$ mK. When the grain size is decreased to the submicron range, its T_c increases by an order of magnitude [8]. It was suggested theoretically that these changes in the electronic and magnetic properties of Pt can be attributed to scatterings at the surface [9]. The static spin susceptibility of an individual Pt grain was found to be strongly reduced by spin-orbital scattering in the presence of surfaces. As the linear dimension of the grain falls below 10 nm, the Rashba effect becomes significant [9]. The reduction of the spin susceptibility disfavors ferromagnetic instability, making superconducting instability preferred over ferromagnetism. On the other hand, spin-orbital scattering time was shown to be proportional to the elastic scattering time [10], suggesting that the presence of the surface tends to enhance spin-orbital coupling. In addition, lattice softening at the surface is expected to lead to enhanced electron-phonon coupling, in particular, when the surface area to volume ratio becomes sufficiently large [11].

These surface induced effects can be explored experimentally by quantum transport measurements – magneto electrical transport measurements exploring the quantum correction to the sample conductance from the quantum interference of the electronic waves. In a weakly disordered metal, quantum interference of electronic waves over a pair of time-reversal paths leads to coherent back scattering of charge carriers [12-14]. The probability for an electron to return to the origin in such a process is twice as great as in classical diffusion, leading to a negative rather than positive quantum correction to the sample conductance. Strong spin-orbital coupling will bring an additional phase of π for the same interference, resulting in a return probability half of that in classical diffusion. The former is known as weak localization (WL) while the latter is called weak antilocalization (WAL) [1,2]. The magnetoresistance (MR) was shown to depend sensitively to spin-orbital coupling, electron-phonon interactions, and magnetic

fluctuations, making quantum transport measurement an effective probe of the electronic and magnetic properties of a weakly disordered metal.

Mesoporous Pt have been synthesized and characterized by microscopy studies [15-18], but the materials are not suitable for transport measurements. The synthesis of metalattices by infiltrating the voids of a close-packed silica nanosphere template (Fig. S1 in Supplemental Material (SM)) by high-pressure confined chemical fluid deposition was recently reported [19]. These metalattices can be thought to possess "meta-atoms", the tetrahedral and octahedral voids in the template, and "meta-bonds", the thin channels connecting the tetrahedral and octahedral voids [20,21]. In comparison with face-centered cubic (fcc) close-packed arrays of nanospheres featuring a surface area to volume ratio of $s = 6/d$, where d is the diameter of the nanosphere, a metalattice featuring an inverse fcc structure has an unprecedentedly high s value of $17.2/d$.

To prepare Pt metalattices, we adapted a metallization chemistry involving (1,5-cyclooctadiene)dimethyl platinum (II) as a Pt precursor pre-dissolved in supercritical CO_2 with a mixture of 20% H_2 in He as a reducing agent [6]. The temperature for both the precursor dissolution and the deposition reaction was 70 °C. Spatial confinement was used to increase the tendency for heterogenous surface nucleation and the growth relative to homogenous nucleation [19]. Spatial confinement on top of the template was found to be critical to the suppression of homogenous reaction and the formation of a (blocking) metal coating on top of the template. Under all three confinement conditions (Fig. S3 in SM), Pt was well infiltrated into the interstitial voids, forming well-connected metalattices. We successfully synthesized Pt metalattices using templates of silica nanospheres with diameters ranging from 30 to 125 nm. The lateral size of the metalattice film is limited only by the size of the reactor, which is on the mm scale. A Pt overlayer co-deposited on top of the metalattice during the Pt nanocasting was removed by reactive ion etching (RIE) before the SEM images were collected. Within a detection limit of 1-2%, no carbon impurities often found in other preparative routes to 3D nanomaterials were detected by XPS in our Pt metalattices (Fig. S4 in SM). The continuous Pt overlay film was removed afterwards, but the SiO_2 spheres were left in this metamaterial of Pt.

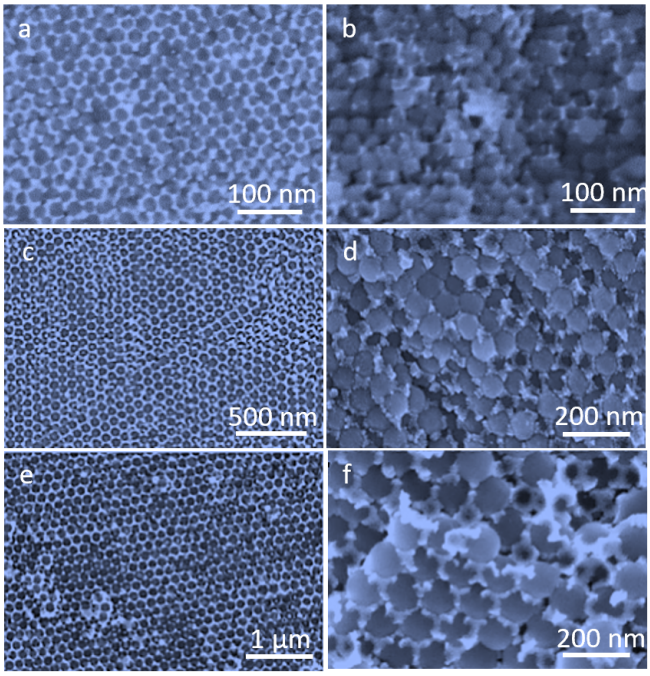

FIG. 1. (Color online) Preparation of metalattices of Pt with a varying periodicity. Scanning electron microscope (SEM) images for 30 nm (a, b), 75 nm (c, d), and 125 nm (e, f) Pt metalattices, showing the top and cross-section view, respectively. All images were taken on samples with silica nanospheres left inside the samples.

In Fig. 1, we show scanning electron microscopy (SEM) images of the top surface and the side view of Pt metalattices prepared in templates formed by silica nanospheres of three different sizes: 30 nm, 75 nm and 125 nm in diameter. The size of nanospheres are checked under SEM and show a standard deviation of up to 5 nm. In images of 30 and 75 nm metalattices, occasional intergrowth and dislocations in the crystal of silica nanosphere can be seen. The 125 nm metalattice, however, appears to be free from such lattice imperfections within the field of view. The cross-sectional images of the Pt filled template indicate that Pt is infiltrated into the template from the top to the bottom, with the thickness of the metalattices up to 1 µm.

We performed detailed structural and chemical characterization of metalattices formed in a 30-nm template. Selected area electron diffraction (SAED) reveals the as-deposited metalattices to consist of polycrystalline Pt (Fig. 2a). Scanning transmission electron microscopy (STEM) and high-angle annular dark-field (HAADF) imaging (Fig. 2b) showed an inverse fcc structure. Energy dispersive X-ray spectroscopy (EDS) mapping of Pt (Fig. 2c) confirms the chemical composition of the network shown in Fig. 2b. Careful inspection of the high resolution TEM (HRTEM) images of a 30 nm Pt metalattice revealed parallel lattice fringes from crystalline grains (data not shown) of a size in the range of 5 - 10 nm. HAADF transmission electron microscope (TEM) image of the cross-section of a 30 nm Pt metalattice over a large length scale (Fig. 2d) suggests long-range alignment of meta-atoms and their good connectivity.

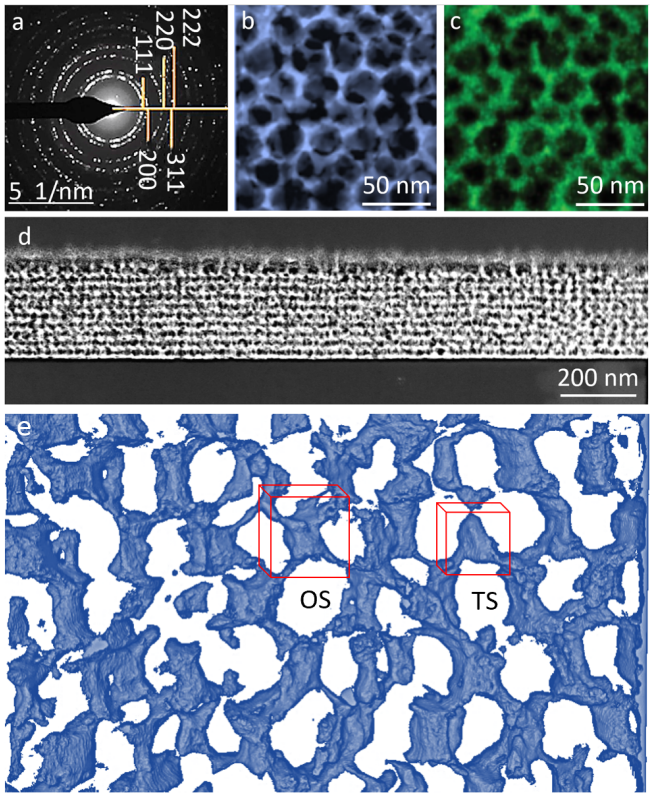

FIG. 2. (Color online) Characterization of 30 nm Pt metalattices. (a) Electron diffraction pattern from transmission microscope (TEM) studies showing that Pt metalattice is polycrystalline. (b) High angle annular dark field (HAADF) STEM image of the cross section of the Pt metalattice. (c) Energy-dispersive X-ray Spectroscopy (EDS) image showing uniform Pt composition in the same area as in (b). (d) Cross sectional TEM shows that Pt metalattice is well ordered over a length scale of 1 μm. (e) HAADF-STEM tomography image of a Pt metalattice, tilted to show the 3D shape of octahedral and tetrahedral site (TS) and octahedral sites (OS). The defects seen in this image were likely introduced by the high-energy focused ion beam preparation of the ultrathin sample for this study.

Data from HAADF-STEM tomographic studies (Fig. 2e) show that the Pt metalattice prepared by infiltrating a template of 30 nm silica nanospheres is nearly void free with the meta-atoms at tetrahedral (TS) and octahedral (OS) sites possessing their sizes and shapes as expected in filled interconnected clusters (Fig. S5 in SM). The linear sizes of the meta-atoms are roughly 7 nm for tetrahedral and 13 nm for octahedral sites, with the bowtie-shaped meta-bonds having a thickness of roughly 2 nm in the thinnest part. The distance between two neighboring octahedral and that between two tetrahedral sites are both 26 nm, and the octahedral and tetrahedral sites are separated by 18 nm. The occasional broken meta-bonds seen in Fig. 2e were likely artifacts introduced by the high-energy focused ion beam preparation of this ultrathin sample.

Metalattices of Pt prepared with a template of 30 nm silica nanospheres were measured down to 2 K. Our measurements revealed metallic behavior in the temperature dependence of the sample resistance, consistent with the expectation of WAL. Without considering the volume of the template, the nominal values of resistivity of the two samples at 2 K were 280 μΩ cm for Sample 1 and 550 μΩ cm for Sample 2, while the scaled values are 179 μΩ cm and 351 μΩ cm, and the residual resistance ratio (RRR) is 1.77

and 1.16 for Sample 1 and Sample 2, respectively (Fig. 3a). Taking into account the volume of template by introducing a scaling factor (see SM) and using the carrier density of the bulk single crystal Pt [23], we found the values for the mean-free path to be 2.23 nm and 1.44 nm, respectively. Because of the unusual sample geometry, it is difficult to calculate the mean-free path accurately.

In Fig. 3b, the MR is shown to be always positive above 1 T. At low magnetic fields, however, MR was found to be positive only below 20 K. As the temperature was raised, the low-field MR was found to become negative within a small temperature window from 20 to 28 K (Fig. 3c). Sample 2 was found to show very similar behavior (Fig. S6 in SM). Negative MR can in principle come from Kondo impurities embedded in a metal [24] or from a ferromagnetic order [25]. Bulk Pt is nearly ferromagnetic. Superparamagnetism was observed in Pt nanoclusters of a size below 3.8 nm protected by capping molecules and monodispersed Pt clusters consisting of 13 atoms in a zeolite [2, 5, 26]. A general survey scan in XPS was acquired and no Fe was detected. The Fe detection limit in our experiment is ~0.2 atom%. Superconducting quantum interference device (SQUID) magnetometry measurements revealed no sign of a ferromagnetic order in the Pt metalattices (data not shown), making the Kondo effect or ferromagnetism unlikely an origin of the observed negative MR.

Effects of WL can lead to negative MR. As pointed above, coherent back scatterings of diffusive charge carriers will lead to a quantum correction to the sample conductivity. Spin-orbital coupling, ferromagnetic fluctuation, and electron-phonon scatterings will be the main sources for the scatterings. The application of the magnetic field will add an additional phase for the quantum interference, changing the value of the quantum correction. Within the theory of WL/WAL, these processes are characterized by three lengths: L_{so}, the dephasing length due to spin-orbital scattering, L_{φ}, the inelastic decoherence length due primarily to the electron-phonon interaction, and L_{MF}, the length characterizing scattering from ferromagnetic fluctuation [1,2]. Spin-orbital coupling yields positive MR while scatterings from ferromagnetic fluctuation and electron-phonon scatterings result in negative MR.

The vast surface area in the 30 nm Pt metalattice will provide sufficiently large surface scattering to enhance the spin-orbital coupling [9]. In addition, given that the sizes of the meta-atoms are roughly 7 nm for tetrahedral and 13 nm for octahedral sites, and size of the meta-bond down to 2 nm in the thinnest part are below or slightly larger than the theoretically predicted threshold, 10 nm, Rashba spin-orbital coupling will also become significant [9]. As a result, strong and positive contribution to MR from spin-orbital contribution is expected. To overcome this enhanced positive contribution to MR so that an overall negative value of MR can be obtained, we must examine contributions from ferromagnetic fluctuation and electron-phonon scatterings. However, as pointed above, the enhancement of the spin-orbital coupling from the presence of the vast surface area in 30 nm metalattices of Pt is expected to suppress ferromagnetic fluctuation, making this source of the negative MR theoretically doubtful. Experimentally, longitudinal MR obtained by aligning the magnetic field with the measurement current is commonly used to gauge how important the ferromagnetic fluctuation is. Unfortunately, it is not possible to align a magnetic field with the current everywhere in a metalattice (Fig. S2 in SM). The above analysis suggests that the enhanced electron-phonon scatterings from the surface, which was predicted theoretically [9] and confirmed by the experimental observation of superconductivity in Pt powders [7, 8], is the only reasonable physical origin for the observed negative MR between 20 – 28 K. The observation of the negative MR at relatively high temperatures provide further supports of this picture as the number of phonons increases with the increasing temperature. It is also reasonable to expect that the negative MR disappears as the temperature increases further because of the loss of the quantum coherence that kills the quantum correction to the sample conductance to begin with.

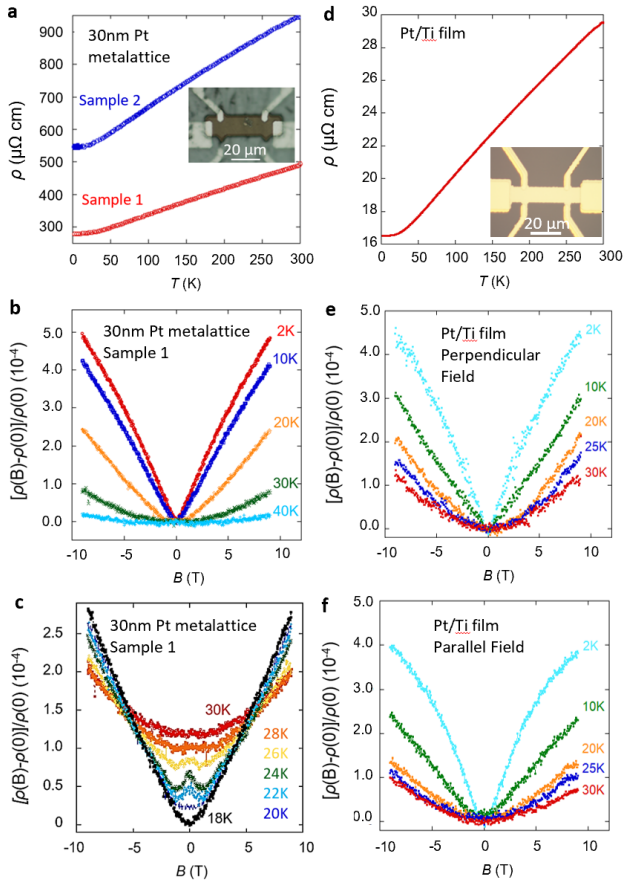

FIG. 3. (Color online) Electrical transport measurements on metalattice and a film of Pt. (a) Temperature dependence of the resistivity of 30 nm Pt metalattices. The inset shows an optical image of a sample. (b) Normalized values of magnetoresistance (MR) at fixed temperatures below 20 K for Sample 1. (c) MR of Sample 1 between 18 and 30 K. The temperatures for the curves from top to bottom are T = 30, 28, 26, 24, 22, 20 and 18 K. All curves except that obtained at 18 K were shifted vertically for clarity. (d) Temperature dependence of the resistivity of a planar film of Pt. A 5-nm-thick Ti underlay was used to promote adhesion. The substrate is Si with 300 nm thermally grown SiO_2. The inset shows an optical image of the device. (e) Values of transverse MR with the field perpendicular to the measurement current and the plane of the film. (f) Values of longitudinal MR with the field parallel to the measurement current.

Theoretical calculations for MR from WL/WAL effects in 3D systems are not nearly as readily available as those for 2D systems. However, they are in the literature [13,14,27]. Importantly, however, all existing theories are formulated for homogeneously disordered systems without dealing with the dominance of the surface scattering and ordered voids encountered in a metalattice sample. The ordered structure featuring strong and specific nanoscale geometrical constraints are expected to have effect on the WL/WAL not found in a homogeneous system. For example, the spin-orbital length is found to be 12 nm in 1D Pt wire [28], comparable to the lateral size of meta-atoms (13 nm / 7 nm) or the length of meta-bonds (18 nm between octahedral and tetrahedral sites) in 30 nm metalattices. Such spatial dispersion of the

diffusion coefficient is not considered in existing WL/WAL theory. A detailed fit of the theory to the magnetic field dependence of MR data was not attempted.

As shown in Fig. 3c, the amplitude of negative magnetoresistivity was found to be around 2.5×10^{-3}, 3.6×10^{-3}, and 1.8×10^{-3} μΩ cm at 1 T at 22, 24, and 26 K, corresponding to a magnetoconductivity of 11, 17, and 5.5 S m^{-1}, respectively, after taking into account the sample volume reduction from the template – An appropriate effective thickness smaller than the nominal thickness of the Pt/SiO_2 nanosphere film was used. Theoretical calculations on the quantum corrections to magnetoresistivity taking into account of both electron-phonon scattering induced dephasing and ferromagnetic fluctuation for a weakly, homogeneously disordered 3D metal can be found in Ref. 27. Assuming a thermal cut-off length and other parameters that are reasonable for our metalattice samples, we calculated the expected magnetoconductivity curve without considering the effect of surface scatterings (see SI). The theoretical curve is close to those we obtained experimentally at low fields. Given that we do expect that the quantum interference effects will be suppressed at sufficiently high magnetic fields, our analysis does suggest that not only the observed negative MR originates from WL/WAL effects, but also that electron-phonon scatterings are primarily responsible for the observed negative MR.

To gain additional physical insights into the observed behavior seen in our 30 nm Pt metalattice, we prepared and measured a reference sample of a planar film of Pt with a thickness of 10 nm. The film was deposited by e-gun evaporation at room temperature. The thickness was chosen as an average of the size of the octahedral and tetrahedral sites. A 5-nm-thick Ti underlayer was deposited on a Si substrate with native oxide to promote adhesion. The residual resistance ratio (RRR) value of this Pt film, 1.7, is very close to that of the Pt metalattice (Fig. 3d). The resistivity of the 10 nm Pt film is more than one order of magnitude lower than in 30 nm metalattice. Note that the use of a 5-nm-thick Ti underlayer should only reduce the overall spin-orbital coupling of the system because of its small Z value in comparison with that of Pt.

Only positive MR was observed in the control sample (Fig. 3e and f). Furthermore, it is seen that the transverse MR is slightly larger than the longitudinal one, consistent with the expectations for a system with strong spin-orbital coupling. It is interesting to note that negative MR has been previously observed in ultrathin Pt films at very low temperatures [29]. However, these ultrathin Pt films (0.6 and 3.2 nm thick) prepared by sputtering onto a Si substrate were very resistive, with a value of resistance per square above 10^5 Ω, which means that the system is beyond weakly localized regime, making the origin of negative MR unclear. Indeed, in another experimental study, ultrathin films of Pt (1.2 to 2.5 nm thick) prepared by evaporation onto a glass substrate with resistance per square ~10^3Ω were found to show positive MR [30]. The observation of the positive MR in our reference sample suggests that the unprecedently large surface area to volume ratio is crucial for the observation of negative MR in 30 nm metalattices.

According to classical Boltzmann transport theory, the transverse MR obtained by aligning the magnetic field normal to the sample current and the plane of the film of a disordered conductor with one type of carriers has a quadratic dependence on the field [31], as seen in bulk Pt [32]. Such conventional quadratic field dependence in MR was indeed observed in 30 nm Pt metalattices above 30 K (Fig. 3c and Fig. S6 in SI). As noted above, we found that the MR depends linearly on magnetic field above 1 T in our 30 nm metalattices of Pt. Interestingly, for the control sample of the film, both field orientations were found to yield very similar linear MR at low temperatures (Figs. 3e and f). These observations suggest that the linear MR is unrelated to the large surface area to volume ratio. We discuss some possible physical origins of linear MR in the SI.

To summarize, results obtained from our quantum transport studies of the metalattice of Pt down to 2 K revealed strong effects of the large surface to area ratio on the properties of Pt metal. The observation of positive MR at low temperature is consistent with the theoretical expectation that the spin-orbital coupling will be enhanced by surface scatterings, which will in turn suppress the ferromagnetic fluctuation seen in bulk Pt. The negative MR observed at low magnetic fields in a narrow temperature window was attributed to the effect of WL/WAL – The negative MR from the surface enhanced electron-phonon scattering in Pt metalattices appeared to dominate the positive MR from the spin-orbital scattering, as expected theoretically. The effect of WL/WAL has never been observed previously in any 3D form of Pt.

Properties found in Pt metalattices as presented above raise the intriguing possibility that 3D nanostructured materials can be engineered for specific properties once appropriate design rules are established. While surfactant or ligand-coated nanoparticles can also be assembled into ordered 3D crystals, they may not have desired homogeneous chemical composition. Mesoporous metals, although nanoscale confined, do not have the structural order and periodicity characteristic of a metalattice. The size, the shape, and chemical composition of the meta-atoms and meta-bonds are uniform over a length scale on the order of millimeters, owing to the void-free infiltration of the metal or semiconductor into the parent silica nanosphere lattice. Combined with the vast and interestingly shaped surface area, these features make metalattices a promising material system to explore in the future. In particular, the enhanced electron-phonon scattering will lead to an enhanced second-order effect – the electron-phonon interaction relevant to the occurrence of superconductivity should also be strengthened. It remains to be seen if these Pt metalattices will exhibit superconductivity at temperatures lower than those reached in the present study.

ACKNOWLEDGEMENTS

We acknowledge useful discussions with Vin Crespi, Chris Giebink, and Mingliang Tian. We thank the Penn State Materials Characterization Lab and Nanofabrication Lab for support in material characterization and sample preparation. This work was supported by the Penn State Center for Nanoscale Science, an NSF-sponsored Materials Science and Engineering Center under award DMR-1420620.

---

[1] H. Ulrichs, V. E. Demidov, S. O. Demokritov, W. L. Lim, J. Melander, N. Ebrahim-Zadeh, and S. Urazhdin, Appl. Phys. Lett. **102**, 132402 (2013).

[2] W. Wendler, T. Herrmannsdörfer, S. Rehmann, and F. Pobell, Europhys. Lett. **38,** 619 (1997).

[3] V. Rodrigues, J. Bettini, P. C. Silva, and D. Ugarte, Phys. Rev. Lett. **91,** 096801 (2003).

[4] G. Y. Guo, S. Murakami, T. W. Chen, and N. Nagaosa, Phys. Rev. Lett. **100**, 096401 (2008).

[5] X. Liu, M. Bauer, H. Bertagnolli, E. Roduner, J. van Slageren, and F. Phillipp, Phys. Rev. Lett. **97,** 253401 (2006).

[6] M. Li, Z. Zhao, T. Cheng, A. Fortunelli, C.-Y. Chen, R. Yu, Q. Zhang, L. Gu, B. Merinov, Z. Lin, E. Zhu, T. Yu, Q. Jia, J. Guo, L. Zhang, W. A. Goddard, Y. Huang, and X. Duan, Science **354**, 1414-1419 (2016).

[7] R. König, A. Schindler, and T. Herrmannsdörfer, Phys. Rev. Lett. **82**, 4528 (1999).

[8] A. Schindler, R. König, T. Herrmannsdörfer, H. F. Braun, G. Eska, D. Günther, M. Meissner, M. Mertig, R. Wahl, and W. Pompe, Europhys. Lett. **58,** 885 (2002).

[9] D. Fay and J. Appel, Phys. Rev. Lett. **89,** 127001 (2002).

[10] R. Meservey and P. M. Tedrow, Phys. Rev. Lett. **41,** 805 (1978).

[11] S. Matsuo, H. Sugiura, and S. Noguchi, J. Low Temp. Phys. **15,** 481 (1974).

[12] A. A. Abrikosov, Fundamentals of the Theory of Metals (North-Holland, 1988).

[13] I. Lifshi͡ts, Quantum Theory of Solids (MIR Publishers, Moscow, 1982)

[14] P. A. Lee and T. V. Ramakrishnan, Rev. Mod. Phys. **57,** 287 (1985).

[15] G. S. Attard, J. M. Corker, C. G. Göltner, S. Henke, and R. H. Templer, Angew. Chemie Int. Ed. English **36,** 1315 (1997).

[16] Y. Yamauchi, A. Sugiyama, R. Morimoto, A. Takai, and K. Kuroda, Angew. Chemie Int. Ed. **47,** 5371 (2008).

[17] H. Wang, H. Y. Jeong, M. Imura, L. Wang, L. Radhakrishnan, N. Fujita, T. Castle, O. Terasaki, and Y. Yamauchi, J. Am. Chem. Soc. **133,** 14526 (2011).

[18] G. L. Egan, J.-S. Yu, C. H. Kim, S. J. Lee, R. E. Schaak, and T. E. Mallouk, Adv. Mater. **12,** 1040 (2000).

[19] Y. Liu, S. Kempinger, R. He, T. D. Day, P. Moradifar, S.-Y. Yu, J. L. Russell, V. M. Torres, P. Xu, T. E. Mallouk, S. E. Mohney, N. Alem, N. Samarth, and J. V. Badding, Nano Lett. **18,** 546 (2018).

[20] J. E. Han and V. H. Crespi, Phys. Rev. Lett. **86,** 696 (2001).

[21] J. E. Han and V. H. Crespi, Phys. Rev. Lett. **89,** 197203 (2002).

[22] J. J. Watkins, J. M. Blackburn, and T. J. McCarthy, Chem. Mater. **11,** 213 (1999)

[23] G. Fischer, H. Hoffmann, and J. Vancea, Phys. Rev. B **22,** 6065 (1980).

[24] J. Kondo, Prog. Theor. Phys. **32,** 37 (1964).

[25] H. Yamada and S. Takada, Prog. Theor. Phys. **48,** 1828 (1972).

[26] Y. Yamamoto, T. Miura, Y. Nakae, T. Teranishi, M. Miyake, and H. Hori, Phys. B Condens. Matter **329–333,** 1183 (2003).

[27] D. V. Baxter, R. Richter, M. L. Trudeau, R. W. Cochrane, and J. O. Strom-Olsen, J. Phys. **50,** 1673 (1989).

[28] Y. Niimi, D. Wei, H. Idzuchi, T. Wakamura, T. Kato, and Y. Otani, Phys. Rev. Lett. **110**, 016805 (2013).

[29] R. S. Markiewicz and L. A. Harris, Surf. Sci. **113,** 531 (1982).

[30] H. Hoffmann, F. Hofmann, and W. Schoepe, Phys. Rev. B **25,** 5563 (1982).

[31] A. B. Pippard, *Magnetoresistance in metals*. (Cambridge University Press, 1989).

[32] L. J. Neuringer, A. J. Perlman, L. G. Rubin, and Y. Shapira, Rev. Sci. Instrum. **42,** 9-14 (1971).